Title

Evaluating the use of Beer's law for estimating light interception in canopy architectures with varying heterogeneity and anisotropy

Authors

Ponce de León, MA
Bailey, BN

Publication Date

2019-08-24

DOI

10.1016/j.ecolmodel.2019.04.010

Peer reviewed

Evaluating the use of Beer's law for estimating light interception in canopy architectures with varying heterogeneity and anisotropy

María A. Ponce de León[a], Brian N. Bailey[a]

[a]*Department of Plant Sciences, University of California, Davis, Davis, CA 95616, USA*

Abstract

Light interception in plant canopies is most commonly estimated using a simple one-dimensional turbid medium model (i.e., Beer's law). Inherent in this class of models are assumptions that vegetation is uniformly distributed in space (homogeneous) and in many cases that vegetation orientation is uniformly distributed (isotropic). It is known that these assumptions are violated in a wide range of canopies, as real canopies commonly have heterogeneity at multiple scales and almost always have highly anisotropic leaf angle distributions. However, it is not quantitatively known under what conditions these assumptions become problematic given the difficulty of robustly evaluating model results for a range of canopy architectures. In this study, assumptions of vegetation homogeneity and isotropy were evaluated under clear sky conditions for a range of virtually-generated crop canopies with the aid of a detailed three-dimensional, leaf-resolving radiation model. Results showed that Beer's law consistently over predicted light interception for all canopy configurations. For canopies where the plant spacing was comparable to the plant height, Beer's law performed poorly, and over predicted daily intercepted sunlight by up to ∼115%. For vegetation with a highly anisotropic leaf inclination distribution but a relatively isotropic leaf azimuth distribution, the assumption of canopy isotropy (i.e., G=0.5) resulted in relatively small errors. However, if leaf elevation and azimuth were

both highly anisotropic, the assumption of canopy isotropy could introduce significant errors depending on the orientation of the azimuthal anisotropy with respect to the sun's path.

Keywords: Beer's law, Heterogeneous canopies, Leaf angle distribution, Light interception, Row orientation

1. Introduction

Solar radiation is a primary driver of most plant biophysical processes, including energy transfer, turbulent transport, evapotranspiration, photosynthesis, and phenology. Fluxes of absorbed radiation in plant canopies have strong gradients in the vertical direction, and potentially in horizontal directions in the case of heterogeneous canopies (Ross, 1981). Capturing these high gradients through direct measurement is often challenging, and therefore models are frequently used to predict absorbed radiative flux distributions.

For practical purposes, relatively simple models are frequently used to estimate light interception in plant canopies. For example, crop models have become important tools for studying agricultural systems (Jones et al., 2017), yet they commonly utilize relatively simple models for light interception given the frequent lack of detailed architectural inputs.

The most commonly used approach for estimating light interception treats the canopy as a homogeneous medium of unresolved vegetation (i.e., a "turbid" medium), which allows for the use of a simple exponential model for radiation attenuation commonly know as Beer's law, Beer-Lambert law, or Beer-Lambert-Bouguer law (Monsi and Saeki, 1953; Lemeur and Blad, 1975; Porter et al., 1993; Sampson and Smith, 1993; Boote and Pickering, 1994; Jones et al., 2003; Lunagaria and Shekh, 2006; Liu et al., 2015). Beer's law calculates the probability of radiation interception as an exponentially increasing function of the leaf area projected in the direction of radiation propagation and the distance travelled through the canopy. Using this approach, light interception can be calculated as

$$I = I_0 \left[1 - \exp\left(-\frac{GL}{\cos\theta_s} \right) \right], \tag{1}$$

where I is the radiation flux intercepted over the depth of the canopy, I_0 is the direct-beam radiation flux on a horizontal surface at the top of the canopy, L is the leaf area index ($\mathrm{m}^2\ \mathrm{m}^{-2}$), and θ_s is the solar zenith angle. G is the fraction of leaf area projected in the direction of the sun, and is defined mathematically as (Ross, 1981)

$$G = \frac{1}{2\pi} \int_{2\pi} \mathrm{g}_L\left(\Omega_L\right) \left|\Omega_s \cdot \Omega_L\right| \mathrm{d}\Omega_L, \tag{2}$$

where Ω_s is a unit vector pointing in the direction of the sun, Ω_L is a unit vector in the direction of the leaf normal, and $g_L(\Omega_L)$ is the probability that a leaf normal is oriented in the direction Ω_L. If g_L is constant for all Ω_L (i.e., leaves have no preferred orientation and are thus isotropic), integration of Eq. 2 yields a value of $G = 0.5$ (Ross, 1981).

The form of Beer's law given in Eq. 1 functions under two main assumptions. The first assumption is that leaf positions are randomly distributed both vertically and horizontally (i.e., homogeneous) in a continuous medium where leaves are relatively small. The second assumption is that leaves absorb all incident radiation (i.e., no scattering or transmission) (Lemeur and Blad, 1975; Larsen and Kershaw Jr, 1996), which may be reasonable for photosynthetically active radiation bands where leaves absorb roughly 90% of incident radiation, but is likely a poor assumption in other bands such as the near-infrared where absorption is low. Equation 1 also requires specification of G, which is most commonly set to be equal to 0.5 based on the assumption that leaves are isotropic (Ross, 1981; Johnson and Thornley, 1984; Sitch et al., 2003; Esprey et al., 2004; Stenberg, 2006).

The assumptions of vegetation homogeneity and isotropy are usually violated in actual plant canopies. Leaf area density typically varies sharply in the vertical direction (Hosoi and Omasa, 2009; Niinemets, 2010; Bailey and Mahaffee, 2017a). Many natural plant canopies have considerable horizontal heterogeneity such as savannas (Chen et al., 2008), or heterogeneity due to natural or man-made disturbances (Levick et al., 2009). Crop canopies also commonly have a sparse, row-oriented configuration that creates high heterogeneity in light interception. Furthermore, it is rare to find canopies with isotropic leaf angle distributions, as this is typically not the most efficient configuration for light interception (Raabe et al., 2015; Bailey and Mahaffee, 2017b).

Despite the known limitations of Beer's law in the above cases, it is still frequently applied in these systems due to its simple, tractable form. However, there is a general lack of quantitative understanding of the errors resulting from the application of these simplified models in various canopy architectures, primarily because it is difficult to quantify light interception from field measurements for a range of architectures (Rosati et al., 2001). The objective of this study is to better understand and quantify errors in modeled radiation absorption under assumptions of vegetation homogeneity or isotropy for various canopy configurations. The authors' hypothesis is that Beer's law will perform well for relatively dense, closed canopies provided that G is specified appropriately. For sparse canopies, it is hypothesized that assumptions of vegetation homogeneity will result in significant model errors, thus necessitating a more complicated model.

Since accurately measuring the distribution of absorbed radiation in space and time is often unfeasible using traditional experimental approaches, a sophisticated 3D radiation model (Bailey, 2018) was used along with virtually-generated canopies to evaluate Beer's law under different simplifying assumptions. Virtual canopies with varying levels of heterogeneity, sparseness, and leaf orientation distributions were generated to evaluate assumptions of vegetation

homogeneity or isotropy in terms of absorption of direct solar radiation. A considerable advantage of using virtually-generated canopies is that the input parameters in Eq. 1 (i.e., G and L) can be calculated exactly from the virtual canopies. When combined with a detailed 3D radiation model, this resulted in a robust means for evaluating the performance of simplified models for a range of canopy architectures.

2. Materials and methods

2.1. Plant geometry

For simulating plant light interactions, detailed 3D geometric models were used to describe the architecture of the canopy. Agricultural crops were chosen for the plant types because: (1) many 3D models are readily available, (2) they have sufficient yet regular heterogeneity that limits the degrees of freedom when generating the canopies, and (3) they represent an economically important practical application of the use of Beer's law. The chosen crop canopies were grape, almond, potato, and corn, which were represented in the 3D model using a mesh of rectangular and triangular elements. To minimize the number of elements needed to describe their complex geometries, images with a transparency channel could be overlaid on these basic elements, where the transparency channel is used to remove a portion of the element's surface (see Suffern, 2007; Bailey, 2018). Virtually-generated plants were either read from a polygon file (corn and potato), or created using the procedural plant generator described by Weber and Penn (1995) (grape and almond).

2.2. Canopy structure

Parameters used to quantify canopy architecture are given in Table 1. The procedural model used to generate the grape and almond plants had a random component to each architectural parameter, making each plant unique. Each corn and potato plant was identical, therefore a random azimuthal rotation was applied to each plant to decrease regularity of the canopy. Plants were placed in a marked row structure to form a canopy. Two grape canopy cases were considered: one with a North-South row orientation (Grape N-S) and one with an East-West row orientation (Grape E-W). Two potato canopies were considered in which plants were arranged in either a East-West row-oriented pattern (Potato-Row), or a uniformly spaced planting pattern (Potato-Uniform). In all cases, the size of the 3D scene was chosen such that further increasing the total number of plants did not have an impact on results.

To test the model in the case of homogeneous and isotropic vegetation, a set of canopies were created with uniformly distributed leaves in space with three different leaf area index values: L =1.5, which consisted of 100,000 leaves; L =3.1, which consisted of 200,000 leaves; and L =6.2, which consisted of 400,000 leaves. The surface area of each leaf was 0.006 m^2. Each leaf angle was set by randomly drawing from a spherical distribution.

Table 1: Parameters used to quantify the structure of the virtually-generated crop canopies.

Case	Plant height (m)	Plant spacing (m)	Row spacing (m)	L (m^2 m^{-2})	Gap fraction
Grape N-S/E-W	2.3	2	2.4	0.9	0.8
Almond	7.6	4.8	6.4	5.1	0.49
Corn	2.4	0.4	1	4.2	0.21
Potato-Uniform	0.8	0.6	0.6	6.5	0.22
Potato-Row	0.8	0.4	0.9	6.5	0.36

To characterize the plant geometry, L and the leaf inclination angle probability density function (PDF) were calculated for all five generated canopies, and the leaf azimuthal angle PDF was calculated for the Grape N-S and Grape E-W cases (all other cases had azimuthal distributions that were close to uniform). The L was calculated by summing the one-sided area of all leaves in the canopy and dividing by the total canopy footprint area. The leaf inclination angle and leaf azimuthal angle were calculated for each of the elements from the surface normal of the leaf, and a PDF was formed by weighting each element's contribution to the PDF by its surface area, then normalizing such that the PDF integrates to unity.

The corn model had predominantly vertically oriented leaves, while the almond and potato models had leaves closer to horizontal on average (Fig. 1). Grape leaf inclination was skewed toward vertical, and leaf azimuth tended to be oriented parallel with the row (Fig. 2), which is supported by previous manual and LiDAR measurements (Bailey et al., 2014; Bailey and Mahaffee, 2017b).

The gap fraction was calculated from the 3D models by computing the fraction of direct sunlight not intercepted when $\theta_s = 0$ (Table 1). Gap fraction values ranged from 80% in the grape canopy cases down to 21% for the corn canopy case. Although both potato canopy cases had the same L, their gap fractions were 22% for uniformly spaced plants and 36% for row-oriented plants.

2.3. One-dimensional model of light interception

A simple 1D model (Eq. 1) was used to calculate hourly light interception, which utilized two different assumptions of canopy structure. The first approach assumed that canopy vegetation is both homogeneous and isotropic. The homogeneous assumption implies that vegetation is randomly distributed in space, which is already inherent in Eq. 1. The isotropic assumption implies that leaves have no preferred orientation, or that the leaf angle PDF is "spherical".

The second approach assumed that leaves are homogeneous but anisotropic. Rather than calculating the leaf angle PDF and integrating according to Eq. 2, the canopy-level $G(\theta_s)$ was calculated directly from the 3D models using a

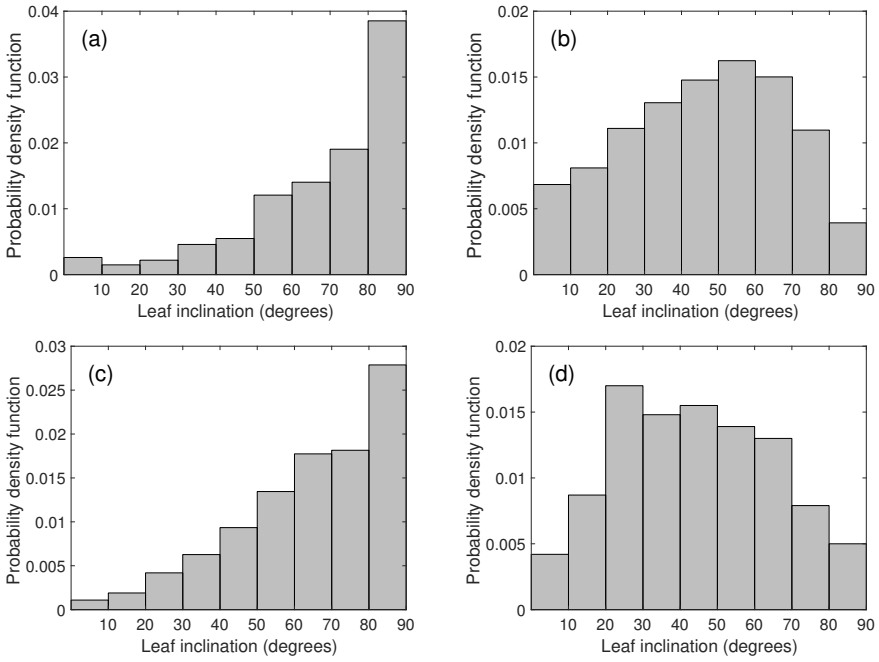

Figure 1: Probability density function of leaf inclination for: (a) Grape N-S/E-W, (b) Almond, (c) Corn, and (d) Potato-Uniform and Potato-Row.

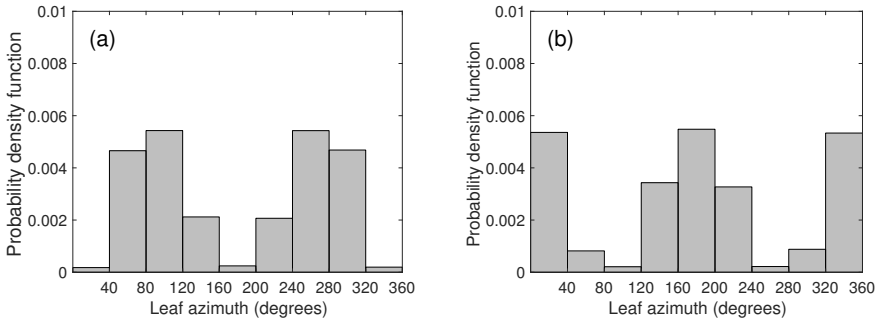

Figure 2: Probability density function of leaf azimuthal angle for Grape (a) N-S and (b) E-W.

weighted average of the projected leaf area fraction according to

$$G(\theta_s) = \frac{\sum_{i=1}^{m} A_i |\vec{n_i} \cdot \vec{v}|}{\sum_{i=1}^{m} A_i}, \tag{3}$$

where m is the total number of geometric elements in the virtual canopy, $\vec{n}_i$

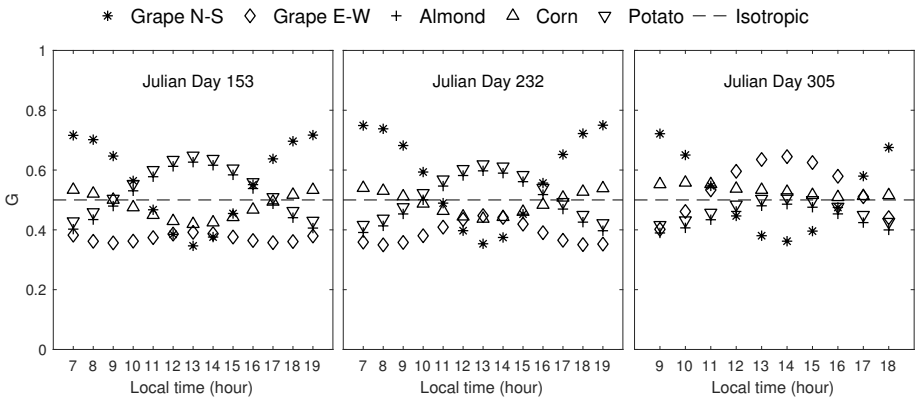

Figure 3: Fraction of leaf area projected in the direction of the sun, G, as a function of time for the virtual canopies.

is a unit vector normal to the surface of the i^{th} geometric element, $\vec{v}$ is a unit vector pointing towards the sun, and A_i is the one-sided surface area of the i^{th} geometric element.

G values for each hour of a diurnal cycle on Julian days 153, 232, and 305 are shown in Fig. 3. For Corn, G does not vary considerably with the position of the sun, whereas the potato and almond cases, have high diurnal variation in G. As Warren Wilson (1960) pointed out, G values intersect at a solar elevation of about 32.5° for azimuthally symmetric vegetation, which corresponds to roughly 8:45 and 17:25 hours on Julian day 153 and 9:20 and 17:00 hours on Julian day 232 in Fig 3. This intersection occurs for the almond, corn, and potato cases, however, because of the highly anisotropic azimuthal leaf distribution of the grape canopies, they do not follow this rule.

In addition to Eq. 1, which assumes vertical homogeneity within the canopy, vertical profiles of hourly absorbed radiation were also calculated by explicitly representing variation of leaf area with height and its corresponding effect on light interception. The radiation flux intercepted over a horizontal layer of thickness Δz at height z within the canopy was calculated according to

$$I(z) = I_0 \left[1 - \exp\left(-\frac{Ga\Delta z}{\cos\theta_s}\right)\right] \exp\left(-\frac{GL_z}{\cos\theta_s}\right), \tag{4}$$

where L_z is the leaf area index between z and the canopy top, and a ($\text{m}^2\ \text{m}^{-3}$) is the one-sided leaf area density of the layer.

The 1D model inherently assumes that leaves absorb all incoming radiation. There is no theoretically consistent means of accounting for reflection and transmission using Eq. 1, as the derivation of Beer's law requires removal of the scattering terms from the radiative transfer equation (Modest, 2013). Several *ad hoc* approaches have been used in previous work to account for transmission

and reflection using some function of the leaf reflectivity (ρ) and transmissivity (τ), of which two are considered here. The first is to multiply the incoming radiation by 1-ρ

$$I = I_0 \left(1 - \rho\right) \left[1 - \exp\left(-\frac{GL}{\cos\theta_s}\right)\right], \tag{5}$$

which assumes that all reflected radiation either exits the canopy or reaches the ground without being re-absorbed and that there is no transmission. The second is to multiply by 1-ρ-τ

$$I = I_0 \left(1 - \rho - \tau\right) \left[1 - \exp\left(-\frac{GL}{\cos\theta_s}\right)\right], \tag{6}$$

which assumes that all reflected and transmitted radiation either exits the canopy or reaches the ground without being re-absorbed.

2.4. Three-dimensional model of light interception

It was assumed that the reference or "true" light interception values were given by the detailed 3D model of Bailey (2018), which explicitly represents radiation absorption by each element in the virtual canopy. The model uses a backward ray-tracing approach that ensures each canopy element adequately samples the sun, and was shown to converge exponentially towards the exact answer as the number of rays was increased (assuming model inputs are specified exactly). The 3D model software and documentation is available though the public GitHub repository `https://www.github.com/PlantSimulationLab/Helios`.

Inputs to the radiation model are the total hemispherical radiative flux (W m^{-2}) of the sun over an arbitrary wavelength band, as well as the reflectivity and transmissivity of each element in the virtual canopy. To test the assumptions of vegetation homogeneity and isotropy, reflectivity and transmissivity were set to 0, which is an assumption implicit in Eq. 1. Separate tests were then performed to examine the effect of reflection and transmission using either Eq. 5 or 6.

For all simulations, the diffuse solar radiation flux was set to 0, which is also implicit in Eq. 1. The number of rays that were sampled on each element was set to 1000 rays. It was verified that further increasing the number of rays had a negligible impact on results. A sample visualization of the 3D distribution of absorbed radiation for the virtual canopy cases is shown in Fig. 4.

Total daily light interception was calculated by linear interpolation of the hourly light interception fluxes. Agreement between the 3D model and simplified 1D models was quantified using the index of agreement (IA; Willmott, 1981), normalized root mean square error (NRMSE), and the coefficient of determination (R^2).

2.5. Radiation input data

The incoming radiation data used to drive the radiation absorption simulations in this study was generated following the REST-2 model of Gueymard

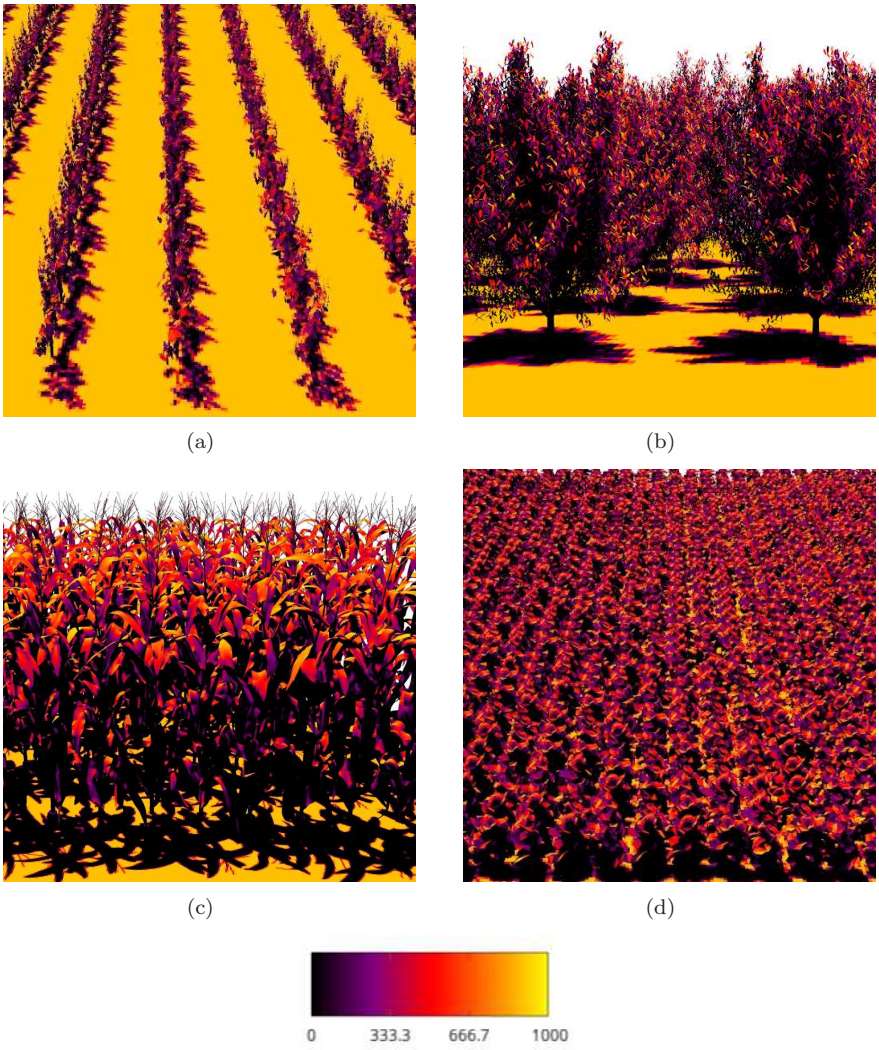

Figure 4: 3D visualization of absorbed radiation flux (W m^{-2}) at 12:00 hours (I_0=928 W m^{-2}, θ_s = 21.5°) on Julian day 153 from: (a) Grape N-S, (b) Almond, (c) Corn, and (d) Potato-Row.

(2008). The hourly incoming radiation was calculated based on the assumed virtual site longitude (121.7405° W), latitude (38.5449° N), offset from UTC (7 hours), atmospheric pressure (101,325 Pa), air temperature near ground level (25°C), atmospheric turbidity coefficient (0.05), relative humidity (50%), and Julian day of the year (153, 232, and 305). It is noted that the precipitable water in the REST-2 model was specified using the model of Viswanadham (1981). The direction of the sun for any time of day at the virtual site was calculated

following the approach outlined by Iqbal (1983).

In cases where scattering was included, two radiative bands were considered - one characteristic of efficient absorption by leaves such as the photosynthetically active band (PAR; 400-700 nm), and another characteristic of high scattering such as the solar near-infrared band (NIR; >700 nm). The total incoming solar flux was partitioned as 47% in the PAR band and 53% in the NIR band. In the PAR band, ρ was set to 0.056 and τ to 0.042, while in the NIR band, ρ was set to 0.425 and τ to 0.334 (Bailey et al., 2014).

3. Results

3.1. Daily total light interception

Results for the daily total light interception on Julian days 153, 232, and 305 are listed in Table 2, and shown graphically in Fig. 5. For the homogeneous canopy cases, very close agreement was found between the 1D and 3D models regardless of L, which indicated that the approach used to compare the 1D and 3D models was consistent and that leaf-scale heterogeneity created by discrete leaf surfaces did not create significant errors.

Cases with relatively high ground cover fractions and uniformly arranged plants showed good agreement between the 1D and 3D models regardless of whether the assumption of leaf isotropy was made. As the canopies became more heterogeneous in space, agreement between the models generally declined. Although Potato-Uniform and Potato-Row had identical leaf area indices and leaf angle distributions, the regular distribution of plants within the canopy in Potato-Uniform resulted in better agreement between the 1D and 3D models compared to Potato-Row. Despite all cases having highly anisotropic leaf inclination distributions, the assumption of leaf anisotropy had relatively small impact for all cases except for the Grape E-W case. Any effects of heterogeneity or anisotropy tended to decrease as the day of year became further away from the summer solstice. Toward the end of the year (day 305), the 1D and 3D models were in fairly good agreement for all canopy cases.

3.2. Hourly light interception

The diurnal flux of radiation intercepted by the canopy for an hourly time step on Julian day 153 is shown in Fig. 6, with corresponding fractions of total radiation intercepted by the canopy shown in Fig. 7. The fraction of total radiation intercepted on Julian day 253 and 305 are shown in Figs. 8 and 9, respectively. For the homogeneous canopy cases, the assumptions of vegetation homogeneity and isotropy were closely satisfied, and therefore, the 1D model was in very good agreement with the 3D model regardless of leaf density (Table 3).

For the crop canopy cases, the 1D model consistently over estimated light interception as compared to the 3D model, except for Grape E-W and Potato-Row on Julian day 305. For all but the grape cases, eliminating the isotropic assumption resulted in little improvement of agreement between the 1D and 3D

Table 2: Daily total light interception (MJ m^{-2} d^{-1}) for the canopies in study

Canopy	Homogeneous and isotropic			Homogeneous and anisotropic			3D model		
	Julian day								
	153	232	305	153	232	305	153	232	305
Grape N-S	296	267	157	293	264	147	229	203	108
Grape E-W	292	264	155	236	227	171	136	150	162
Almond	607	529	256	618	535	255	380	348	225
Corn	588	514	253	574	505	254	485	475	250
Potato-Uniform	622	539	257	628	544	257	544	499	250
Potato-Row	622	539	257	628	544	257	422	404	257
Homogeneous canopy									
L=1.5	406	362	203	406	362	203	408	360	203
L=3.1	545	480	245	545	479	245	550	482	245
L=6.2	619	538	257	619	538	257	619	537	257

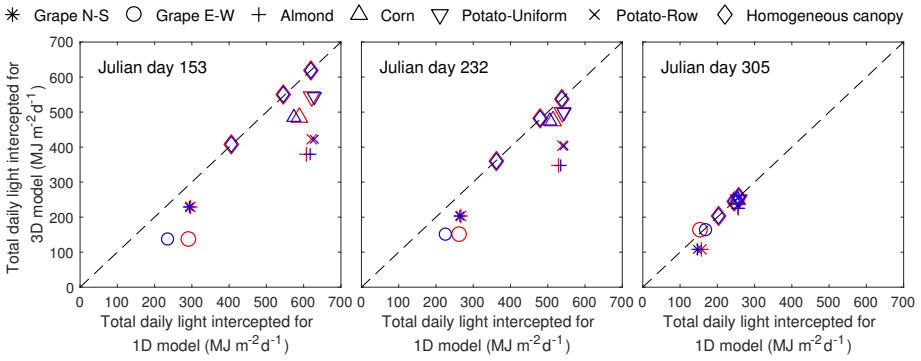

Figure 5: Comparison of daily total light interception predicted by the 1D vs. 3D models for homogeneous and isotropic (red), and for homogeneous but anisotropic (blue) canopies (for data values see Table 2). Dotted line is 1:1 agreement.

models, indicating that errors arose primarily from heterogeneity in these cases. For the Grape N-S, Almond, and Potato cases, errors between the 1D and 3D models were largest near midday when sunlight could most readily reach the ground by penetrating through gaps in vegetation. For Grape E-W, the largest discrepancies occurred at early and late times of the day. The effect of row orientation on diurnal interception patterns for the grape cases was dramatic, as this completely changed the character of interception at different times of the year (see Figs. 6, 7, 8, 9). The potato cases also illustrated the pronounced effect of heterogeneity in planting pattern on diurnal interception.

3.3. Vertical profiles of hourly absorbed radiation

Figure 10 depicts vertical profiles of the absorbed radiation flux at 8:00, 10:00, and 12:00 hours on Julian day 153 for Grape N-S, Grape E-W, Almond,

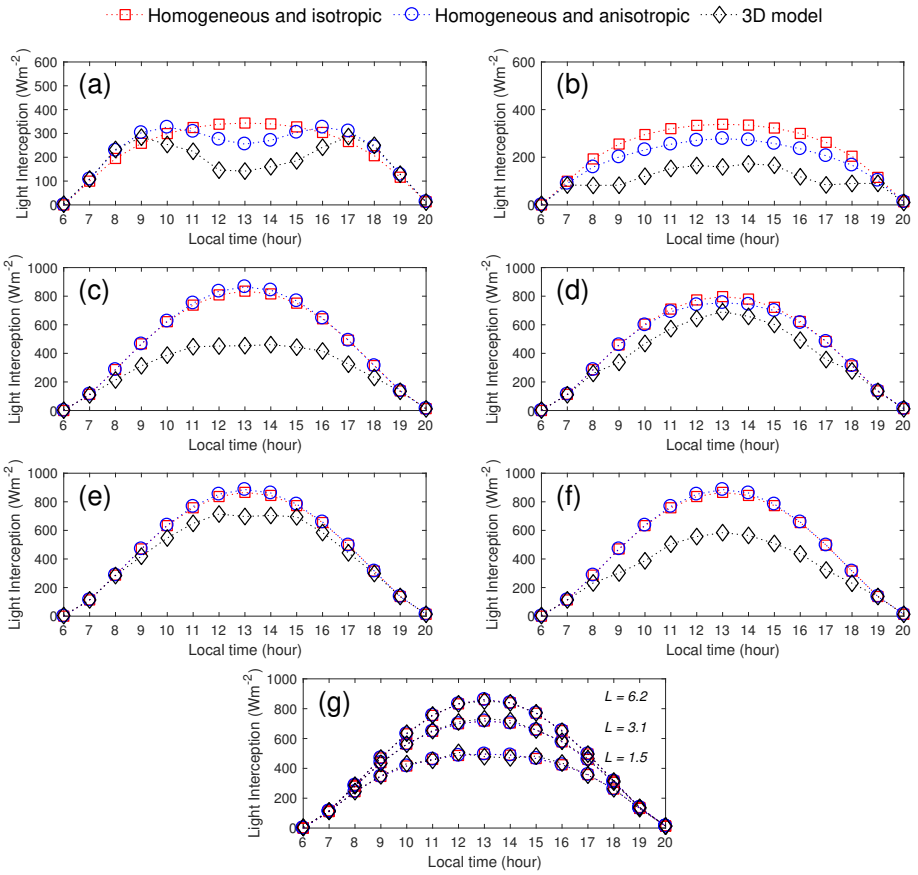

Figure 6: Comparisons of the 1D model and 3D model for hourly flux of light interception on Julian day 153 from: (a) Grape N-S, (b) Grape E-W, (c) Almond, (d) Corn, (e) Potato-Uniform, (f) Potato-Row, and (g) homogeneous canopies with three different L values. Both homogeneous and isotropic and homogeneous and anisotropic refer to the 1D model.

and Corn. Errors in absorbed fluxes for Grape N-S were relatively consistent with height, where errors at a given height were most closely related to the magnitude of the absorbed flux at that height. This was also roughly the case for Almond, except that there was the potential for some under estimation of absorption in the lower canopy when the 1D model was used, which was most pronounced for larger solar zenith angles. For Grape E-W, the 1D model tended to shift the peak in the absorbed flux deeper into the canopy, which was most pronounced for larger solar zenith angles.

In the corn canopy, the vertical pattern in radiation interception differed significantly between the 1D and 3D models. There were up to 50% differences between 1D and 3D fluxes at a given vertical level, with irregular patterns of over or under estimation. In the lower canopy, there was a peak in absorption

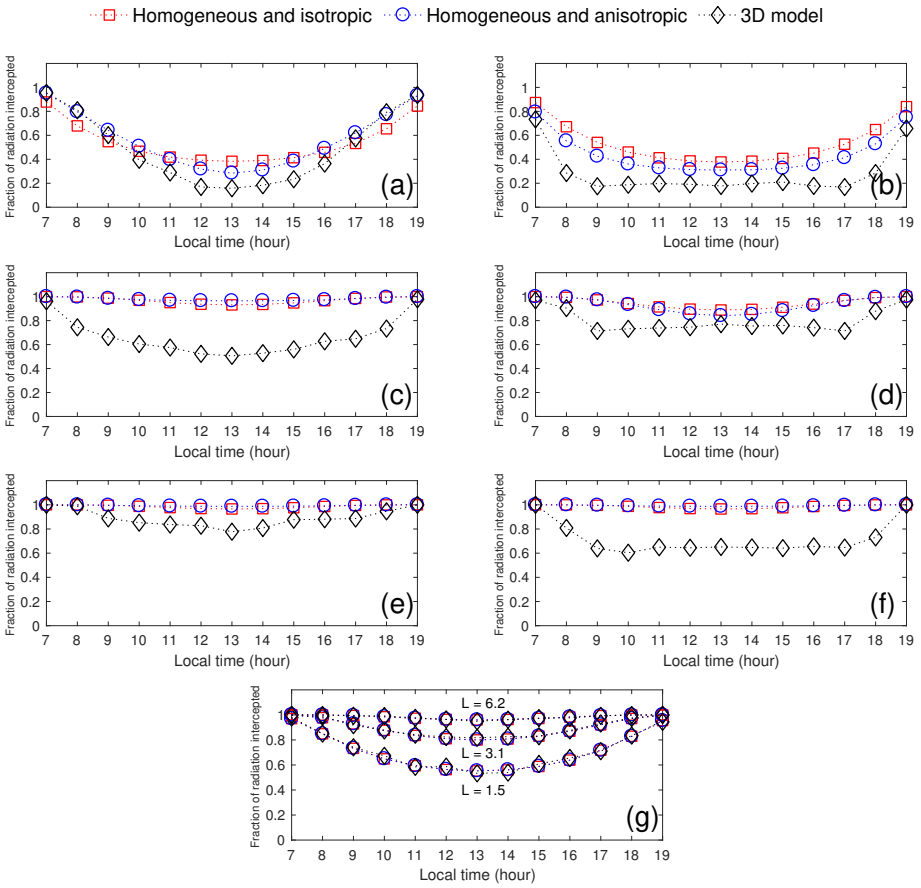

Figure 7: Comparisons of the 1D model and 3D model of hourly light interception, expressed as a fraction of direct-beam radiation, on Julian day 153 for: (a) Grape N-S, (b) Grape E-W, (c) Almond, (d) Corn, (e) Potato-Uniform, (f) Potato-Row, and (g) homogeneous canopies with three different L values. Both homogeneous and isotropic and homogeneous and anisotropic refer to the 1D model.

in the 3D model, which was largely absent in the 1D model, leading to under prediction of absorption by the 1D model in the lower canopy. This is likely due to the substantial over prediction of absorption by the 1D model in the upper canopy, which removes the necessary energy needed to produce a secondary peak in absorption in the lower canopy.

3.4. Impact of scattering

Total daily light interception for Julian day 153 is shown in Fig. 11 for different assumptions regarding radiation scattering, which is given by either Eq. 1 (Fig. 11a; no scattering), Eq. 5 (Fig. 11b; only reflection), or Eq. 6 (Fig. 11c; reflection and transmission). It is important to note that for the homogeneous

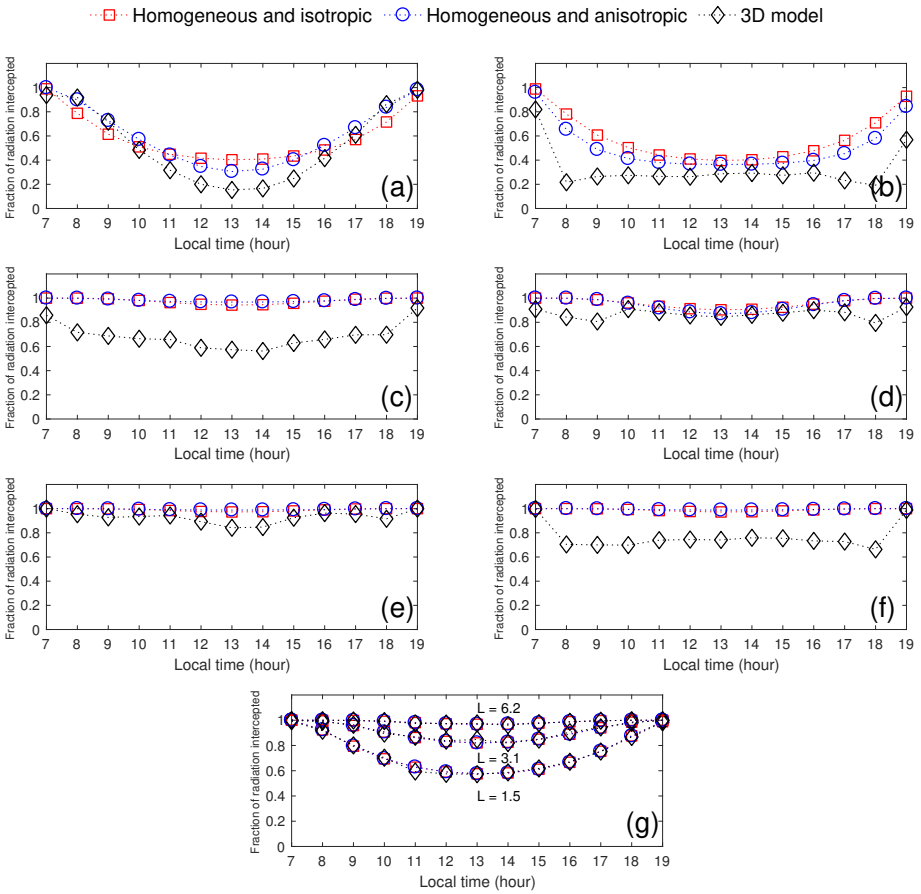

Figure 8: Same as Fig. 7 except for Julian day 232.

canopy cases, errors in Fig. 11 are due only to effects of scattering, as it was shown in Fig. 5 that agreement between the 1D and 3D models was excellent when leaves were black. For the crop canopy cases, errors in Fig. 11 are due to the combined effect of scattering and heterogeneity, which makes these results somewhat difficult to interpret.

As evidenced by the homogeneous canopy cases, the impact of scattering was minimal for the PAR band, and thus most of the errors in the heterogeneous crop canopy cases were due to heterogeneity and not scattering. In the NIR band, scattering caused very large errors when the standard 1D model was used, with all cases over estimating absorption by more than 100%. Accounting for reflection using Eq. 5 removed much of this energy, but still resulted in significant over estimation of absorbed radiation. This approach creates offsetting errors in which absorption is over estimated because transmission is not accounted for, but there is simultaneous under estimation due to the assumption that

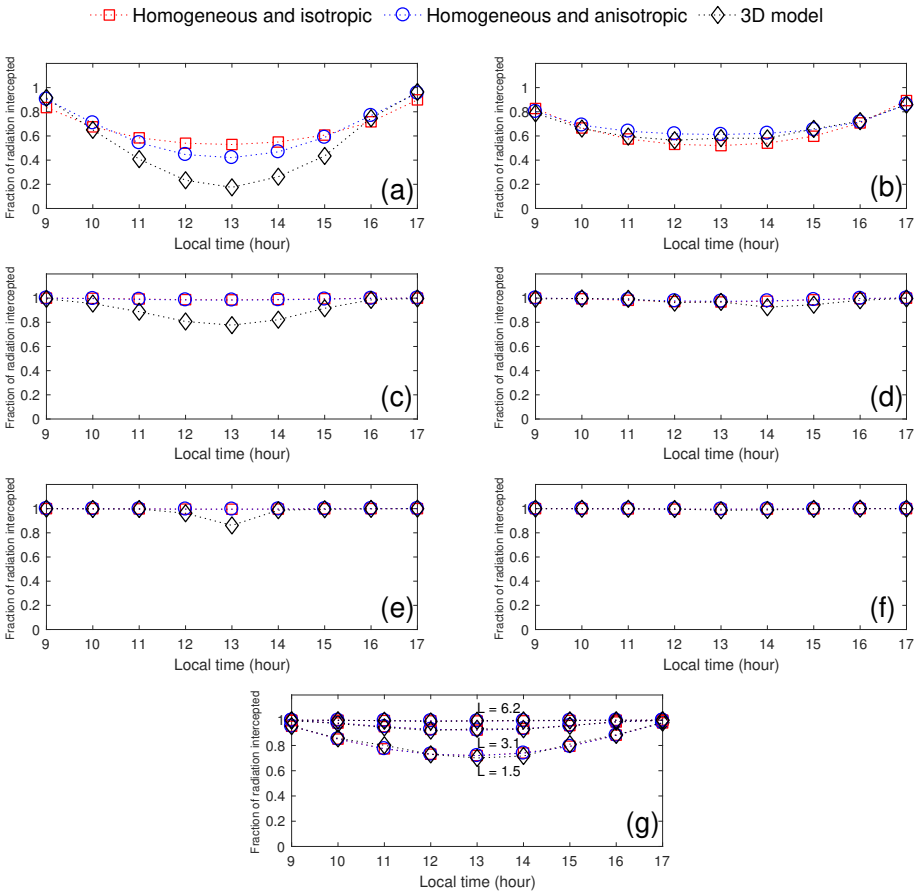

Figure 9: Same as Fig. 7 except for Julian day 305.

all reflected radiation either reaches the ground or is reflected back to the sky (but the net result is over estimation). Accounting for both reflection and transmission using Eq. 6 caused net under estimation of the total absorbed flux. This is because Eq. 6 assumes that all reflected and transmitted radiation radiation either reaches the ground or is reflected back to the sky, thus overall absorption is under estimated.

4. Discussion

4.1. Effect of leaf angle distribution (anisotropy)

Overall, anisotropy in leaf inclination had a relatively small effect on errors resulting from the application of Beer's law in cases when leaf azimuth was uniformly distributed (Almond, Corn, and Potato). The grape cases, which had

Table 3: Model performance measures comparing results from the 1D and the 3D model for hourly light interception for the virtually-generated canopies based on data for hourly light interception (a graphical depiction of the data is shown in Fig. 6).

3D vs.1D (Homogeneous and isotropic)									
	Julian Day 153			Julian Day 232			Julian Day 305		
Canopy	R^2	IA	NRMSE	R^2	IA	NRMSE	R^2	IA	NRMSE
Grape N-S	-0.35	0.78	0.29	-0.14	0.81	0.29	-0.59	0.79	0.30
Grape E-W	-6.39	0.65	0.41	-0.32	0.81	0.31	0.98	0.99	0.5
Almond	-0.95	0.8	0.27	0.02	0.87	0.23	0.9	0.98	0.1
Corn	0.82	0.96	0.12	0.98	1.00	0.05	1.00	1.00	0.02
Potato-Uniform	0.90	0.98	0.09	0.97	0.99	0.06	0.99	1.00	0.04
Potato-Row	0.02	0.87	0.22	0.68	0.94	0.16	1.00	1.00	0.00
Homogeneous canopy									
L=1.5	1.00	1.00	0.02	1.00	1.00	0.02	1.00	1.00	0.02
L=3.1	1.00	1.00	0.01	1.00	1.00	0.01	1.00	1.00	0.01
L=6.2	1.00	1.00	0.00	1.00	1.00	0.00	1.00	1.00	0.00
3D vs.1D (Homogeneous and anisotropic)									
Canopy	R^2	IA	NRMSE	R^2	IA	NRMSE	R^2	IA	NRMSE
Grape N-S	0.32	0.88	0.22	0.42	0.89	0.22	0.19	0.87	0.27
Grape E-W	-2.08	0.73	0.32	0.40	0.89	0.22	0.99	1.00	0.04
Almond	-1.17	0.79	0.27	-0.07	0.86	0.23	0.90	0.98	0.1
Corn	0.86	0.97	0.11	0.99	1.00	0.04	1.00	1.00	0.02
Potato-Uniform	0.87	0.98	0.10	0.96	0.99	0.06	0.99	1.00	0.04
Potato-Row	-0.06	0.86	0.22	0.66	0.94	0.16	1.00	1.00	0.00
Homogeneous canopy									
L=1.5	1.00	1.00	0.02	1.00	1.00	0.02	1.00	1.00	0.02
L=3.1	1.00	1.00	0.01	1.00	1.00	0.01	1.00	1.00	0.01
L=6.2	1.00	1.00	0.00	1.00	1.00	0.00	1.00	1.00	0.00

high anisotropy in both the leaf inclination and azimuth distributions, did incur significant errors due leaf anisotropy for the 1D model.

If leaf azimuth is uniformly distributed, this effectively reduces the impact of anisotropy in leaf inclination on the projected area fraction G. Since a leaf with a certain elevation angle could be parallel to the sun at one azimuth and perpendicular to the sun at another, an integration over all azimuths can smear out the effects of leaf inclination alone.

As in the virtual canopies of this study, field measurements have shown that leaf inclination distributions are usually highly anisotropic (Niinemets, 1998, 2010; Raabe et al., 2015; Bailey and Mahaffee, 2017b). The azimuthal distribution of leaves may be strongly anisotropic within a single plant (Bailey and Mahaffee, 2017b), but for relatively dense canopies, the azimuthal distribution is often fairly isotropic (Ross, 1981). In these cases, the assumption of leaf isotropy is likely to result in minimal errors. However, sparse, row-oriented crops such as vineyards may have highly anisotropic azimuthal distributions (Bailey and Mahaffee, 2017b), in which case it may be necessary to explicitly calculate G based on measurements. These types of canopies are becoming increasingly prevalent in agricultural applications (e.g., apples, olives; Connor, 2006; Lauri, 2009), due in part to the improved access to mechanical harvesters that a trellised or hedgerow canopy provides.

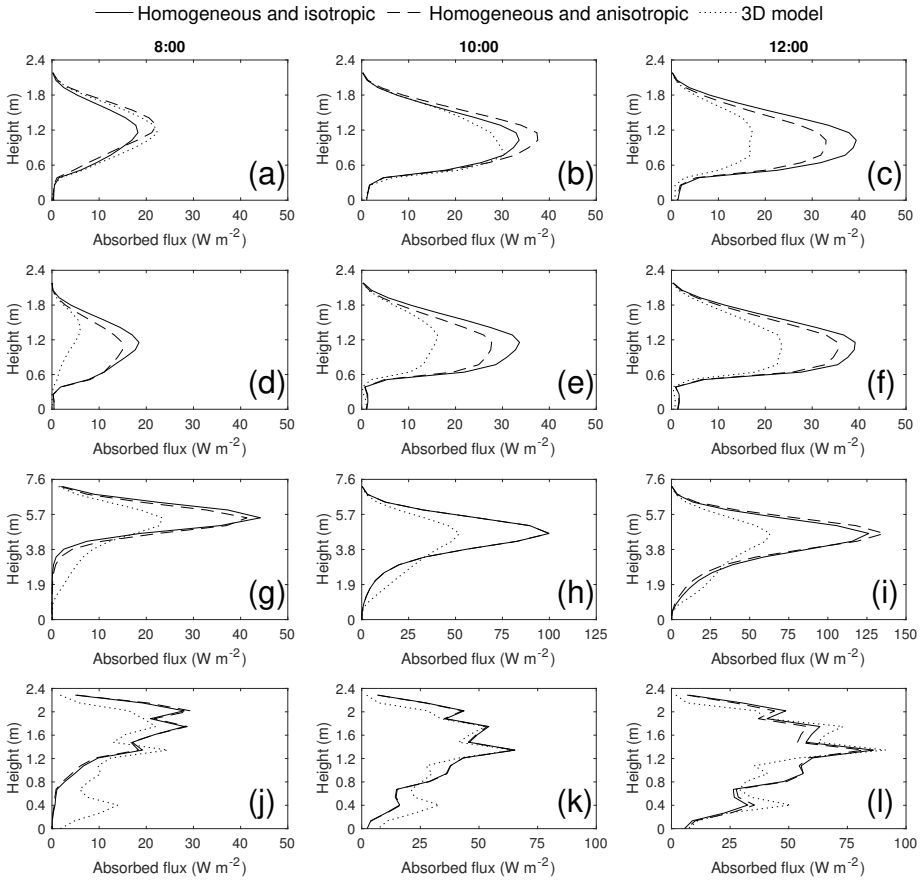

Figure 10: Vertical profile of absorbed radiation from Grape N-S (a, b, c); Grape E-W (d, e, f); Almond (g, h, i); and Corn, (j, k, l) on Julian day 153. Columns correspond to 8:00 (θ_s=66°), 10:00 (θ_s=43°), and 12:00 (θ_s=21°) hours for each crop.

4.2. Effect of plant spacing (horizontal heterogeneity)

Plant spacing and the resulting heterogeneity had the most pronounced effect on errors resulting from the use of Beer's law. For the Grape N-S case, the assumption of homoogeneity resulted in an overestimation of the total daily absorbed radiation by 28%, 30%, and 36% on Julian days 153, 232, and 305, respectively, with larger instantaneous over estimation near midday. For the Grape E-W case, the assumption of homogeneity also resulted in overestimating the total daily absorbed radiation by 74%, 51%, and 5% on Julian days 153, 232, and 305, respectively. This was not simply an effect related to L, as was illustrated by the two potato cases. By simply rearranging the potato plants from a uniformly spaced into a row-oriented configuration, errors in the 1D model increased substantially.

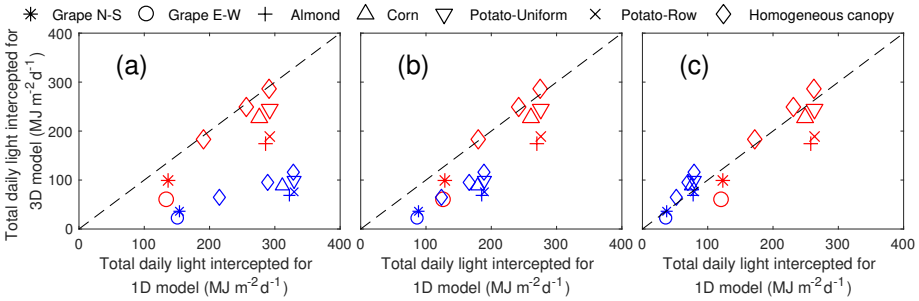

Figure 11: Daily total light interception for homogeneous and isotropic canopies in the PAR band (red) and NIR (blue) for different assumptions regarding radiation scattering based on a) Eq. 1; leaf absorb all incoming radiation, b) Eq. 5, and c) Eq. 6. Dotted line is 1:1.

It is possible that the effect of horizontal heterogeneity can vary in the vertical direction, which appeared to be the case with the Corn canopy. This significantly altered the performance of the 1D model at any given height, although the canopy was dense enough overall that the 1D model performed well when predicting whole-canopy radiation absorption. This could have important implications if the radiation model is coupled with other biophysical models such as a photosynthesis model. The response of photosynthesis to light is nonlinear and asymptotic (Taiz and Zeiger, 2014), so although whole-canopy absorption may be well-represented in some cases by a 1D horizontally homogeneous model, it is unclear if that will result in significant errors in total photosynthetic production given the nonlinearity of its response to light.

A limitation of this study is that results are only applicable under clear sky conditions. However, results can provide some insight regarding diffuse sky conditions by simultaneously considering all canopy geometries and simulated sun angles. Under a uniformly overcast sky, equal energy originates from all directions. A particular combination of sun angle and leaf orientation bias was required in order to observe a pronounced effect of leaf anisotropy. Thus, for diffuse solar conditions, it is speculated that the impact of leaf anisotropy will be decreased. Sun angle had an important effect on the instantaneous impact of leaf heterogeneity, and most commonly it was observed that low sun angles resulted in a decreased impact of heterogeneity. Therefore, it is likely that highly diffuse conditions will reduce the impact of heterogeneity near midday because a significant fraction of incoming radiation will originate from directions nearer to the horizon.

Estimating light interception with Beer's law is based on the assumption that canopies are homogeneous. This inherently means that the rate of radiation attenuation along a given path is linearly related to the flux at that location. As the canopy becomes sparse, there are pathways for radiation propagation that allow radiation to penetrate the entire canopy without any probability of interception, which fundamentally violates the assumptions behind Beer's law

or a turbid medium. Therefore, the non-random leaf dispersion in canopies limits the ability of Beer's law to link light interception to simple bulk measures of plant architecture.

It is well-known that this heterogeneity or "clumping" of vegetation usually results in decreased radiation interception as compared with an equivalent homogeneous canopy. A common means of dealing with this problem without significantly increasing model complexity is to add a "clumping coefficient" Ω to the argument of the exponential function in Beer's law (Nilson, 1971; Smith et al., 1993; Kucharik et al., 1999). While this is a simple and practical means of reducing the amount of radiation attenuation predicted by Beer's law, the challenge in applying the clumping coefficient approach is that Ω is a complex function of nearly every applicable variable (Chen et al., 2008), and thus is it is difficult to mechanistically specify. Another approach is to use a model that explicitly resolves plant-level heterogeneity (e.g., Norman and Welles, 1983; North, 1996; Bailey et al., 2014), as it may not be necessary to explicitly resolve every leaf if within-plant heterogeneity is small.

4.3. Effect of row orientation

Row orientation played an important role when estimating light interception from Beer's law, particularly when the rows were widely spaced. For sparse, row-oriented canopies, the effective path length of the sun's rays through vegetation can change dramatically with changes in sun azimuth. For East-West rows, absorption is significantly reduced early and late in the day because the rows are close to parallel with the sun's rays, whereas North-South rows are perpendicular to the sun at this time. As the day of year progresses further from the summer solstice, the sun spends more time closer to the horizon and thus the impact of heterogeneity in an East-West row orientation increased. For the East-West row configuration, $G(\theta_s)$ and light interception were surprisingly constant throughout much of the day, which resulted in 41% and 36% less absorption on Julian days 153 and 232, respectively, compared to North-South rows. This has important practical implications for agricultural design applications. In some climates, it may be desirable to maximize sunlight interception, whereas in others it may be desirable to mitigate effects of excess sunlight to reduce temperatures and water use.

4.4. Effect of light scattering

Despite the simplified assumptions in Beers law regarding scattering, there was good agreement between predicted radiation interception using the 1D and 3D models in the PAR band. Scattering did not significantly influence light interception in this band because most of the incident radiation received by individual leaves was absorbed. However, in the NIR band, scattering introduced significant over estimation of absorption using the standard 1D model, since leaves are poor absorbers in this band. Using an *ad hoc* correction to account for reflection only reduced this over estimation of absorption. An additional correction to account for both reflection and transmission resulted in over correction, and a net under prediction of total radiation absorption.

5. Conclusion

The objective of this work was to evaluate common assumptions used in estimating radiation absorption in plant canopies, namely assumptions of homogeneity or isotropy of vegetation. Our results demonstrated that for relatively dense canopies with azimuthally symmetric leaves, a 1D model that assumes homogeneity and isotropy of vegetation generally produced relatively small errors. As plant spacing became large, the assumptions of homogeneity break down and model errors became large. In the case of a vineyard with rows oriented in the East-West direction, errors in daily intercepted radiation were up to $\sim 70\%$ due to heterogeneity alone, with much larger instantaneous errors occurring during the day. If leaves were highly anisotropic in the azimuthal direction, there was also the potential for large errors resulting from the assumption of vegetation isotropy which had the potential to increase errors above 100%. Day of year had an impact on model errors, which was that overall errors tended to decline with time from the summer solstice.

In cases of canopies where the plant spacing starts to approach the plant height, it is likely necessary to use a plant-resolving radiation model in order to avoid substantial over prediction of absorbed radiative fluxes. Additionally, if vegetation is highly anisotropic in terms of both elevation and azimuthal angle distributions, it is also likely necessary to explicitly calculate the projected area fraction $G(\theta_s)$ based on measurements and the instantaneous position of the sun.

Acknowledgements

Financial support of this work was provided by the American Vineyard Foundation grants 2016-1825/2017-1825, and the USDA National Institute of Food and Agriculture Hatch project 1013396.

References

Bailey, B.N., 2018. A reverse ray-tracing method for modelling the net radiative flux in leaf-resolving plant canopy simulations. Ecol. Model. 368, 233–245.

Bailey, B.N., Mahaffee, W.F., 2017a. Rapid, high-resolution measurement of leaf area and leaf orientation using terrestrial LiDAR scanning data. Meas. Sci. Technol. 28, 064006.

Bailey, B.N., Mahaffee, W.F., 2017b. Rapid measurement of the three-dimensional distribution of leaf orientation and the leaf angle probability density function using terrestrial lidar scanning. Remote Sens. Environ. 193, 63–76.

Bailey, B.N., Overby, M., Willemsen, P., Pardyjak, E.R., Mahaffee, W.F., Stoll, R., 2014. A scalable plant-resolving radiative transfer model based on optimized GPU ray tracing. Agric. For. Meteorol. 198-199, 192–208.

Boote, K., Pickering, N., 1994. Modeling photosynthesis of row crop canopies. HortScience 29, 1423–1434.

Chen, Q., Baldocchi, D., Gong, P., Dawson, T., 2008. Modeling radiation and photosynthesis of a heterogeneous savanna woodland landscape with a hierarchy of model complexities. Agric. For. Meteorol. 148, 1005 – 1020.

Connor, D.J., 2006. Towards optimal designs for hedgerow olive orchards. Aust. J. Agric. Res. 57, 1067–1072.

Esprey, L., Sands, P., Smith, C., 2004. Understanding 3-PG using a sensitivity analysis. Forest Ecol. Manag. 193, 235 – 250.

Gueymard, C.A., 2008. REST2: High-performance solar radiation model for cloudless-sky irradiance, illuminance, and photosynthetically active radiation - Validation with a benchmark dataset. Solar Energy 82, 272–285.

Hosoi, F., Omasa, K., 2009. Estimating vertical plant area density profile and growth parameters of a wheat canopy at different growth stages using three-dimensional portable lidar imaging. ISPRS J. Photogramm. Remote Sens. 64, 151 – 158.

Iqbal, M., 1983. An Introduction to Solar Radiation. Academic Press, Burlington. 408 pp.

Johnson, I., Thornley, J., 1984. A model of instantaneous and daily canopy photosynthesis. J. Theor. Biol. 107, 531 – 545.

Jones, J., Hoogenboom, G., Porter, C., Boote, K., Batchelor, W., Hunt, L., Wilkens, P., Singh, U., Gijsman, A., Ritchie, J., 2003. The DSSAT cropping system model. Eur. J. Agron. 18, 235 – 265.

Jones, J.W., Antle, J.M., Basso, B., Boote, K.J., Conant, R.T., Foster, I., Godfray, H.C.J., Herrero, M., Howitt, R.E., Janssen, S., Keating, B.A., Munoz-Carpena, R., Porter, C.H., Rosenzweig, C., Wheeler, T.R., 2017. Brief history of agricultural systems modeling. Agric. Syst. 155, 240 – 254.

Kucharik, C.J., Norman, J.M., Gower, S.T., 1999. Characterization of radiation regimes in nonrandom forest canopies: theory, measurements, and a simplified modeling approach. Tree Physiol. 19, 695–706.

Larsen, D.R., Kershaw Jr, J.A., 1996. Influence of canopy structure assumptions on predictions from Beer's law. A comparison of deterministic and stochastic simulations. Agric. For. Meteorol. 81, 61–77.

Lauri, P.E., 2009. Developing a new paradigm for apple training. The Compact Fruit Tree 42, 17–19.

Lemeur, R., Blad, B.L., 1975. A critical review of light models for estimating the shortwave radiation regime of plant canopies, in: Developments in Agricultural and Managed Forest Ecology. Elsevier. volume 1, pp. 255–286.

Levick, S.R., Asner, G.P., Kennedy-Bowdoin, T., Knapp, D.E., 2009. The relative influence of fire and herbivory on savanna three-dimensional vegetation structure. Biol. Cons. 142, 1693 – 1700.

Liu, T., Gu, L., Dong, S., Zhang, J., Liu, P., Zhao, B., 2015. Optimum leaf removal increases canopy apparent photosynthesis, ^{13}C-photosynthate distribution and grain yield of maize crops grown at high density. Field Crops Res. 170, 32–39.

Lunagaria, M., Shekh, A., 2006. Radiation interception, light extinction coefficient and leaf area index of wheat (*Triticum avestum* L.) crop as influenced by row orientation and row spacing. J. Agric. Sci. 2, 43–54.

Modest, M.F., 2013. Radiative Heat Transfer. Academic press, Waltham, MA. 904 pp.

Monsi, M., Saeki, T., 1953. The light factor in plant communities and its significance for dry matter production. Jpn. J. Bot. 14, 22–52.

Niinemets, Ü., 1998. Adjustment of foliage structure and function to a canopy light gradient in two co-existing deciduous trees. Variability in leaf inclination angles in relation to petiole morphology. Trees 12, 446–451.

Niinemets, Ü., 2010. A review of light interception in plant stands from leaf to canopy in different plant functional types and in species with varying shade tolerance. Ecol. Res. 25, 693–714.

Nilson, T., 1971. A theoretical analysis of the frequency of gaps in plant stands. Agric. Meteorol. 8, 25–38.

Norman, J., Welles, J., 1983. Radiative transfer in an array of canopies 1. Agron. J. 75, 481–488.

North, P.R., 1996. Three-dimensional forest light interaction model using a Monte Carlo method. IEEE Trans. Geosci. Remote Sens. 34, 946–956.

Porter, J., Jamieson, P., Wilson, D., 1993. Comparison of the wheat simulation models AFRCWHEAT2, CERES-Wheat and SWHEAT for non-limiting conditions of crop growth. Field Crops Res. 33, 131–157.

Raabe, K., Pisek, J., Sonnentag, O., Annuk, K., 2015. Variations of leaf inclination angle distribution with height over the growing season and light exposure for eight broadleaf tree species. Agric. For. Meteorol. 214-215, 2–11.

Rosati, A., Badeck, F., DeJong, T., 2001. Estimating canopy light interception and absorption using leaf mass per unit leaf area in *Solanum melongena*. Ann. Bot. 88, 101–109.

Ross, J., 1981. The Radiation Regime and Architecture of Plant Stands. Dr. W. Junk Publishers, The Hague, The Netherlands. 424 pp.

Sampson, D.A., Smith, F., 1993. Influence of canopy architecture on light penetration in lodgepole pine (*Pinus contorta* var. *latifolia*) forests. Agric. For. Meteorol. 64, 63–79.

Sitch, S., Smith, B., Prentice, I., Arneth, A., Bondeau, A., Cramer, W., Kaplan, J., Levis, S., Lucht, W., Sykes, M., Thonicke, K., Venevsky, S., 2003. Evaluation of ecosystem dynamics, plant geography and terrestrial carbon cycling in the LPJ dynamic global vegetation model. Global Change Biol. 9, 161–185.

Smith, N., Chen, J., Black, T., 1993. Effects of clumping on estimates of stand leaf area index using the LI-COR LAI-2000. Can. J. For. Res. 23, 1940–1943.

Stenberg, P., 2006. A note on the G-function for needle leaf canopies. Agric. For. Meteorol. 136, 76 – 79.

Suffern, K.G., 2007. Ray Tracing from the Ground Up. A K Peters/CRC Press, Boca Raton, FL. 784 pp.

Taiz, L., Zeiger, E., 2014. Plant Physiology and Development. Sinauer. 761 pp.

Viswanadham, Y., 1981. The relationship between total precipitable water and surface dew point. J. Appl. Meteorol. 20, 3–8.

Warren Wilson, J., 1960. Inclined point quadrats. New Phytol. 59, 1–7.

Weber, J., Penn, J., 1995. Creation and rendering of realistic trees, in: Proceedings of the 22Nd Annual Conference on Computer Graphics and Interactive Techniques, ACM. pp. 119–128.

Willmott, C.J., 1981. On the validation of models. Physical Geography 2, 184–194.